

Developing a Neural Network for the Identification of EMIC Wave Events

Nyssa S. S. Capman¹, Laura E. Simms², and Mark J. Engebretson³

¹University of Minnesota

²Augsburg University

³Department of Physics, Augsburg University

September 11, 2023

Abstract

A supervised convolutional neural network (CNN) was developed to automatically identify electromagnetic ion cyclotron (EMIC) wave events from spectrograms. These events have usually been identified manually, which can be a time-consuming process. Statistical analyses of larger datasets would be facilitated if this process were simplified. The neural network model was trained on spectrogram images from the Halley magnetometer station that had been manually identified as either containing or not containing an EMIC wave event anywhere in the spectrogram. This model was tested on an unseen set of spectrograms, achieving a perfect true positive rate of 1. Size, time, frequency, and pixel color information was extracted from each identified event and exported into a spreadsheet for easier analysis. This method has the capability of reducing time and effort required to identify important spectrogram features by hand. Such an automated method could be applied to other space weather data stored in spectrograms.

Hosted file

972311_0_art_file_11336646_s07m4p.docx available at <https://authorea.com/users/658668/articles/662921-developing-a-neural-network-for-the-identification-of-emic-wave-events>

Developing a Neural Network for the Identification of EMIC Wave Events

Nyssa S. S. Capman¹, Laura E. Simms^{2,3}, Mark J. Engebretson²

¹Department of Mechanical Engineering, University of Minnesota, Twin Cities, Minneapolis, MN, USA

²Department of Physics, Augsburg University, Minneapolis, MN, USA

³Department of Climate and Space Sciences and Engineering, University of Michigan, Ann Arbor, MI, USA

Key Points

- Automatic identification of EMIC wave events in spectrograms is accomplished with an image classifying convolutional neural network
- Information about the size, time and frequency range, and power of each event is produced and output to a spreadsheet for analysis
- The method applied to 3 years of spectrograms from the Halley, Antarctica ground magnetometer station gives a true positive rate of 1

Abstract

A supervised convolutional neural network (CNN) was developed to automatically identify electromagnetic ion cyclotron (EMIC) wave events from spectrograms. These events have usually been identified manually, which can be a time-consuming process. Statistical analyses of larger datasets would be facilitated if this process were simplified. The neural network model was trained on spectrogram images from the Halley magnetometer station that had been manually identified as either containing or not containing an EMIC wave event anywhere in the spectrogram. This model was tested on an unseen set of spectrograms, achieving a perfect true positive rate of 1. Size, time, frequency, and pixel color information was extracted from each identified event and exported into a spreadsheet for easier analysis. This method has the capability of reducing time and effort required to identify important spectrogram features by hand. Such an automated method could be applied to other space weather data stored in spectrograms.

Plain language summary

Electromagnetic ion cyclotron waves in the earth's magnetosphere are often represented in spectrogram images, and wave events have usually been identified by a human examining the images by eye. To speed up the data collection process, an automatic method to extract information about each event has been developed.

35 1. Introduction

36 Space weather wave events have usually been identified by examining spectrograms by
37 eye and recording the frequency and time ranges of notable wave events. This process is time-
38 consuming and slows down the analysis of space weather data even as the amount of available
39 data has increased. Previous work has sought to develop methods to automate this process,
40 including use of Fourier Transform methods to analyze the power spectral density of wave data
41 (Bortnik et al., 2007; Kim et al., 2018; Di Matteo et al., 2021; Inglis et al., 2015; Inglis et al.,
42 2016; Murphy et al., 2020), discrete wavelet transforms (Omondi et al., 2022), and trigger
43 algorithms that look for cases of simultaneity between two or more variables known to correlate
44 with the events of interest (Carson et al., 2013). Few studies have explored the use of image
45 analysis and object identification algorithms to automatically detect wave events directly from
46 spectrogram images (Antonopoulou et al., 2022). However, neural network image analysis is a
47 common method of object identification in remote sensing, used to locate and count craters
48 (DeLatte et al., 2019), map water levels (Mandlbürger et al., 2021), and map coral reefs (Li et al.,
49 2020) among other applications. In all of these examples, the basic task is the same as is needed
50 for space weather spectrograms: identifying shapes in image data and recording their location
51 and characteristics such as size and color.

52 This work shows a convolutional neural network (CNN) developed to identify
53 electromagnetic ion cyclotron (EMIC) wave events in spectrograms measured at the Halley,
54 Antarctica ground magnetometer station between November 2006 and December 2009. The
55 algorithm identifies and records both the time frame and frequency range of each EMIC wave
56 event. The algorithm also outputs a rough estimate for wave power by recording the ratio of
57 pixels in several color bins to the total number of pixels in the event. This aids the human
58 researcher to filter which events should be further examined, or which events should be included
59 in statistical analyses depending on particular research needs.

60

61 2. Model Training and Event Extraction

62 2.1. Model Training

63 A convolution neural network (CNN) was trained using the open-source PyTorch
64 framework in Python (Paszke et al., 2019). A set of 1130 spectrograms from the Halley,
65 Antarctica magnetometer station spanning November 2006 to December 2009 were used to train
66 and test the model. These were manually divided into three classes: “no signals” (483
67 spectrograms), “broadband signals” (324 spectrograms), or “EMIC events” (323 spectrograms).
68 The entire dataset was split into training and test sets in a 70:30 ratio. This was done using
69 stratified sampling in order to maintain the same overall class distribution in each set. The CNN
70 was trained on the training set, and then tested on the “unseen” spectrograms in the test set. The
71 predicted classes were compared to the true classes and a confusion matrix was produced from
72 which various metrics including the overall accuracy and the true positive rates of each class
73 were calculated. Fifty epochs were used to train the models. This number was chosen by
74 examining the training and validation loss, which did not show significant decreases after this

75 point. The CNN consisted of a linear layer, a Tanh activation layer, a second linear layer, and
76 finally a log softmax layer. A batch size of 64 was used. The Python code used to perform this
77 model training has been uploaded to a Zenodo repository (Capman, 2023).

78 **2.2. Event Extraction**

79 After model testing, a Laplacian of Gaussian (LoG) “blob detection” algorithm was
80 applied to only the spectrograms classified as containing events (Python library scikit-image, van
81 der Walt et al., 2014). This algorithm produces circles indicating the location of identified events
82 in pixels. A lookup table was created to relate the pixel locations with the time and frequency
83 information on the x- and y-axes in the spectrograms. This lookup table depends on all
84 spectrograms input into the algorithm having the same layout, dimensions, and axis limits. The
85 identified events are automatically recorded in a spreadsheet which contains the approximate
86 frequency and time frame of the events. This method determines the frequency and time frame of
87 each event by recording the coordinates of the left-, right-, top-, and bottom-most edges of the
88 circle produced by the LoG method. As the LoG identification circles do not always precisely
89 encircle each event, these edges are only estimates. However, they do give a general location in
90 each axis. Also recorded is the total number of pixels in each event circle and the number of
91 pixels in each event circle belonging to each of six color bins (white, red, orange, yellow, green,
92 and blue/black). These color bins were defined in relation to the colors used for plotting the wave
93 power, and as such, the ratio of pixels in each color bin to total pixels in the event circle can be
94 used as a rough estimate of the average power of each EMIC event. The total number of pixels in
95 each event circle gives a rough estimate of the size of each EMIC event. These two pieces of
96 information can help the user to determine which events are worth investigating.

97

98 **3. Classification and Event Extraction Results**

99 Three metrics are used to evaluate the success of the classification model: accuracy, true
100 positive rate (TPR), and Heidke Skill Score (HSS). The accuracy is simply the ratio of correct
101 predictions to total number of predictions. The TPR is calculated as TP/P , where TP is the
102 number of true positives predicted and P is the total number of positives. Finally, the HSS is a
103 measure of how well a model performed relative to the success of a random chance model
104 (Heidke, 1926; calculations as in Ganushkina et al., 2015). The HSS can take values between
105 negative infinity and +1, with +1 indicating a perfect prediction, 0 indicating that the model
106 performed no better than random chance, and negative values indicating that the model
107 performed worse than random chance. The model shown in the confusion matrix of Figure 1 has
108 an accuracy of 86.4%, an HSS of 0.738, and most importantly a true positive rate of $TPR = 1$,
109 when the “EMIC event” class is defined as the positive class, and both “no signals” and
110 “broadband signals” as the negative classes. A TPR of 1 means that we correctly identified
111 events 100% of the time. The accuracy and HSS weight false positives and false negatives
112 equally. We consider the cost of false positives (i.e. a spectrogram with no event being identified
113 as containing an event) to be much less than the cost of a false negative (i.e., missing an event).
114 Therefore, the most important metric for this type of identification problem is the TPR.

115 The LoG algorithm identified larger events well. The algorithm also tended to identify
116 many small and/or weak features that were not of interest, which were filtered out by a minimum
117 radius cutoff. However, this cutoff requires some optimization to balance filtering out
118 unimportant features with removing features of interest that happen to fall under the radius
119 cutoff. For example, in Figure 2, Blobs 1 and 6 do not indicate EMIC events of interest and
120 ideally would have been filtered out. However, increasing the minimum radius cutoff to exclude
121 Blobs 1 and 6 would also have excluded Blob 4 which has the same radius as Blobs 1 and 6, but
122 which contains a weak event of possible interest. This tradeoff is specific to each user’s needs
123 and the characteristics of each dataset.

124 It is important to note that broadband signals are only filtered out on a whole-spectrogram
125 basis by the previous CNN step. For example, Blob 5 in Figure 2 is broadband but was still
126 identified as a possible event. As this spectrogram had a strong event, it was classified into the
127 “event” category despite the presence of broadband elsewhere in the spectrogram. The user must
128 determine which identified blobs are useful and which are broadband based on size and overall
129 color/wave power. Despite this drawback, the CNN/LoG combined method greatly reduces the
130 work necessary to sort through spectrograms, and greatly limits the number of spectrograms to
131 be examined by eye.

132

133 **4. Discussion**

134 One improvement needed for this method is in identifying true EMIC events in the
135 presence of broadband signals in the blob detection algorithm. Currently, broadband is filtered
136 out on a whole-spectrogram basis by the CNN classification. The model tends to classify
137 spectrograms with large, clear events into the “EMIC event” class, regardless of the presence of
138 broadband signal elsewhere in the spectrogram. Once these spectrograms are processed by the
139 LoG blob detection algorithm, broadband signals are identified and recorded alongside the true
140 EMIC events, and it is not always obvious from the spreadsheet output which events are
141 broadband and which are true EMIC events. Conversely, the model classifies most spectrograms
142 with strong broadband into the “broadband signal” class, regardless of the presence of smaller
143 EMIC events, and as such these EMIC events are missed. Typically, broadband signals are
144 identified by the LoG algorithm as being much larger than most EMIC events, since the
145 broadband signals cover a larger portion of the spectrogram in the frequency axis. Based on this
146 fact, the user may be able to filter out broadband signals by applying a maximum radius cutoff
147 for each blob. However, this may also eliminate very large EMIC events which are especially
148 important for analysis, and also not be capable of filtering out smaller broadband blobs, such as
149 Blob 5 in Figure 2. Therefore, such a solution has a high potential cost. Further work is needed to
150 improve the discrimination between true EMIC events and broadband signals.

151 In this study, we opted to divide the data into 3 classes (“no signals”, “broadband
152 signals”, and “EMIC events”). This improved the model success, since otherwise broadband
153 signals were often confused with EMIC events. Another choice is to divide the data into 2
154 classes: “no signals”, and “EMIC events”. In this case, the user would have the option to alter the

155 prediction threshold, making it more or less likely for a given spectrogram to be classified into
156 either class. The softmax layer outputs a predicted probability that a given spectrogram is of one
157 or the other class. The default classification threshold choice is 0.5: spectrograms with
158 probabilities greater than or equal to 0.5 are placed in the positive class (“EMIC event”), and
159 those with probabilities less than 0.5 are placed in the negative class (“no signals”). However, if
160 there is a class imbalance in the dataset, or if one or the other misclassification is more costly, a
161 threshold other than 0.5 might be appropriate, weighting more heavily towards the positive or
162 negative classes. Finding an optimal threshold may be aided with the use of a ROC curve.
163 However, we ultimately determined that dividing this data into three classes produced better
164 results than to use two classes, regardless of threshold optimization.

165

166 **5. Conclusions**

167 The CNN/LoG combined method described here greatly reduces the time and effort
168 required to identify spectrogram features by hand and could also be applied to other space
169 weather data stored in spectrograms. With appropriate optimization, the method could eventually
170 be used to rapidly produce a dataset of event statistics from a large set of spectrograms with little
171 to no input from the human user.

172

173 **Acknowledgements**

174 N.S.S.C. was supported by the National Science Foundation (NSF) through the Graduate
175 Research Fellowship Program (GRFP) program. EMIC wave activity data were obtained from
176 the induction coil magnetometer located at the Halley, Antarctica, British Antarctic Survey
177 (BAS) ground station at L-shell 4.6. This work was supported by NSF Grant AGS-2013648.

178

179 **Data Availability Statement**

180 Spectrograms from the Halley, Antarctica ground magnetometer station are available at
181 <http://space.augsburg.edu/searchcoil/index.html>. The Python code used to train and test the CNN
182 models, as well as the Halley, Antarctica spectrograms used for training are available at
183 <https://doi.org/10.5281/zenodo.8280090>.

184

185 **References**

186 Antonopoulou, A., Balasis, G., Papadimitriou, C., Boutsis, A. Z., Rontogiannis, A., Koutroumbas,
187 K., ... & Giannakis, O. (2022). Convolutional Neural Networks for Automated ULF Wave
188 Classification in Swarm Time Series. *Atmosphere*, 13(9), 1488.
189 <https://doi.org/10.3390/atmos13091488>

190

191 Bortnik, J., Cutler, J. W., Dunson, C., & Bleier, T. E. (2007). An automatic wave detection
192 algorithm applied to Pc1 pulsations. *Journal of Geophysical Research: Space Physics*, 112(A4).
193 <https://doi.org/10.1029/2006JA011900>

194

195 Capman, N. S. S. (2023). Python Code to Train a Neural Network for the Identification of EMIC
196 Wave Events in Spectrograms. (Version 1.0) [Software]. Zenodo.
197 <https://doi.org/10.5281/zenodo.8280090>

198

199 Carson, B. R., Rodger, C. J., & Clilverd, M. A. (2013). POES satellite observations of EMIC-
200 wave driven relativistic electron precipitation during 1998–2010. *Journal of Geophysical*
201 *Research: Space Physics*, 118(1), 232-243. <https://doi.org/10.1029/2012JA017998>

202

203 DeLatte, D. M., Crites, S. T., Guttenberg, N., & Yairi, T. (2019). Automated crater detection
204 algorithms from a machine learning perspective in the convolutional neural network era.
205 *Advances in Space Research*, 64(8), 1615-1628.

206

207 Di Matteo, S., Viall, N. M., & Kepko, L. (2021). Power spectral density background estimate
208 and signal detection via the multitaper method. *Journal of Geophysical Research: Space Physics*,
209 126(2). <https://doi.org/10.1029/2020JA028748>

210

211 Ganushkina, N. Y., Amariutei, O. A., Welling, D., & Heynderickx, D. (2015). Nowcast model
212 for low-energy electrons in the inner magnetosphere. *Space Weather*, 13(1), 16-34.

213

214 Heidke, P. (1926). Measures of success and goodness of wind force forecasts by the gale-
215 warning service. *Geogr. Ann.*, 8, 301–349. doi: [https://doi.org/10.1080/](https://doi.org/10.1080/20014422.1926.11881138)
216 [20014422.1926.11881138](https://doi.org/10.1080/20014422.1926.11881138)

217

218 Inglis, A. R., Ireland, J., Dennis, B. R., Hayes, L., & Gallagher, P. (2016). A large-scale search
219 for evidence of quasi-periodic pulsations in solar flares. *The Astrophysical Journal*, 833(2), 284.
220 <http://dx.doi.org/10.3847/1538-4357/833/2/284>

221

222 Inglis, A. R., Ireland, J., & Dominique, M. (2015). Quasi-periodic pulsations in solar and stellar
223 flares: Re-evaluating their nature in the context of power-law flare Fourier spectra. *The*
224 *Astrophysical Journal*, 798(2), 108. <http://dx.doi.org/10.1088/0004-637X/798/2/108>

225

226 Kim, H., Hwang, J., Park, J., Bortnik, J., & Lee, J. (2018). Global characteristics of
227 electromagnetic ion cyclotron waves deduced from Swarm satellites. *Journal of Geophysical*
228 *Research: Space Physics*, 123(2), 1325-1336. <https://doi.org/10.1002/2017JA024888>

229

230 Li, J., Knapp, D. E., Fabina, N. S., Kennedy, E. V., Larsen, K., Lyons, M. B., ... & Asner, G. P.
231 (2020). A global coral reef probability map generated using convolutional neural networks.
232 *Coral Reefs*, 39, 1805-1815. doi: <https://doi.org/10.1007/s00338-020-02005-6>

233

234 Mandlbürger, G., Kölle, M., Nübel, H., & Soergel, U. (2021). BathyNet: A deep neural network
235 for water depth mapping from multispectral aerial images. *PFG–Journal of Photogrammetry,*
236 *Remote Sensing and Geoinformation Science*, 89(2), 71-89. doi: [https://doi.org/10.1007/s41064-](https://doi.org/10.1007/s41064-021-00142-3)
237 [021-00142-3](https://doi.org/10.1007/s41064-021-00142-3)

238

239 Murphy, K. R., Inglis, A. R., Sibeck, D. G., Watt, C. E. J., & Rae, I. J. (2020). Inner
240 magnetospheric ULF waves: The occurrence and distribution of broadband and discrete wave
241 activity. *Journal of Geophysical Research: Space Physics*, 125(9), e2020JA027887.
242 <https://doi.org/10.1029/2020JA027887>

243

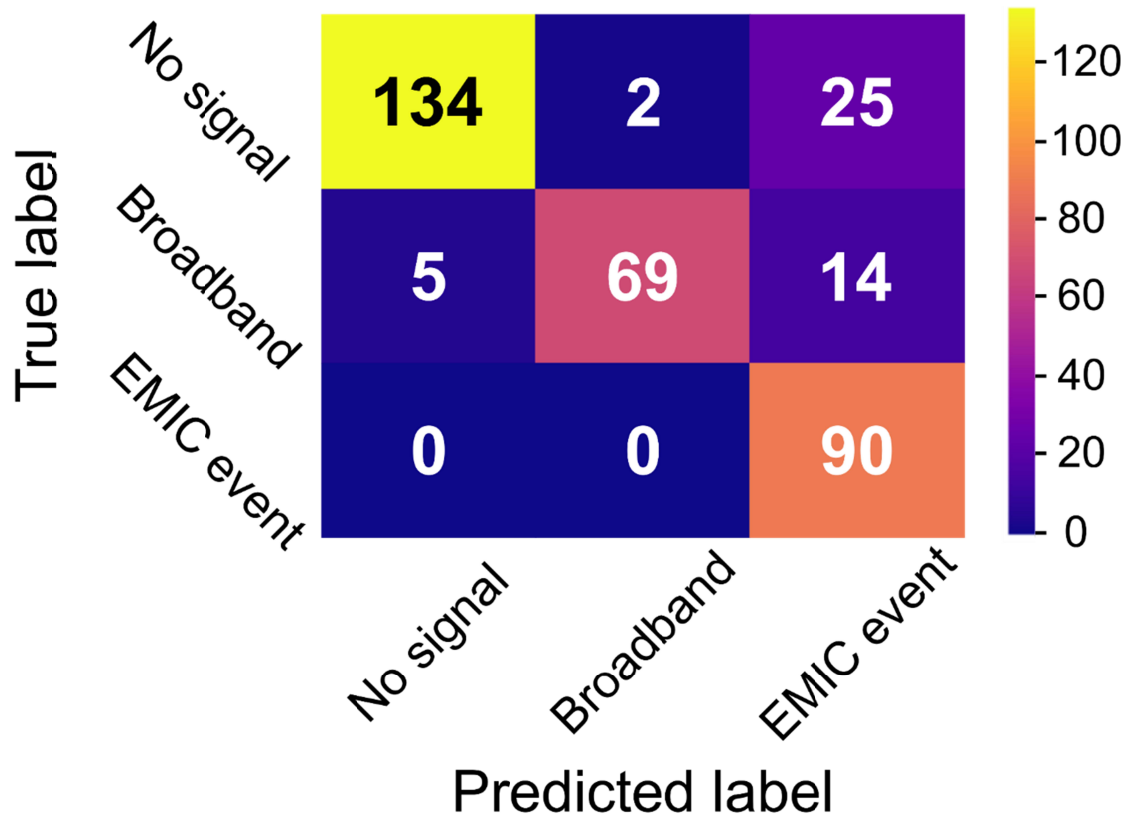
244 Omondi, S., Yoshikawa, A., Zahra, W. K., Fathy, I., & Mahrous, A. (2022). Automatic detection
245 of auroral Pc5 geomagnetic pulsation using machine learning approach guided with discrete
246 wavelet transform. *Advances in Space Research*. <https://doi.org/10.1016/j.asr.2022.06.063>

247

248 Paszke, A., Gross, S., Massa, F., Lerer, A., Bradbury, J., Chanan, G., et al. (2019). Pytorch: An
249 imperative style, high-performance deep learning library. *Advances in neural information*
250 *processing systems*, 32. <https://doi.org/10.48550/arXiv.1912.01703>

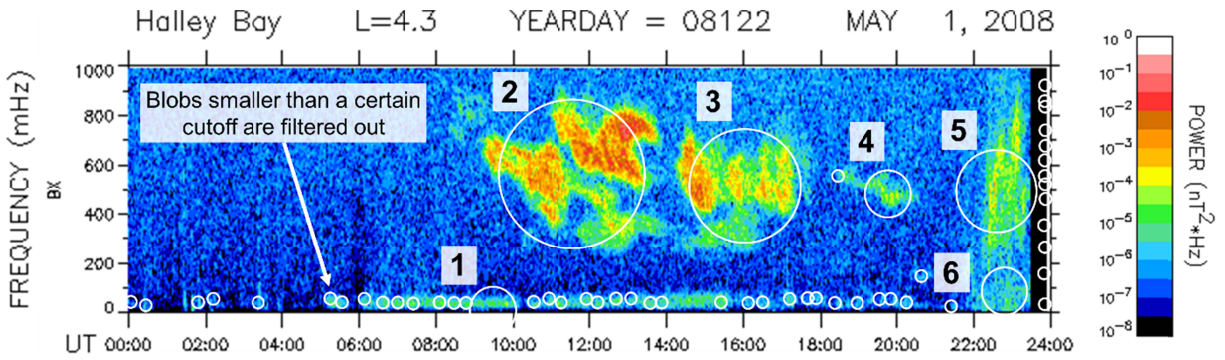
251

252 Van der Walt, S., Schönberger, J. L., Nunez-Iglesias, J., Boulogne, F., Warner, J. D., Yager, N.,
253 ... & Yu, T. (2014). scikit-image: image processing in Python. *PeerJ*, 2, e453.
254 <https://doi.org/10.7717/peerj.453>



255 Figure 1. Confusion matrix for the CNN model showing true and predicted class labels for each
 256 spectrogram in the test set. Considering the “EMIC event” class as the positive class, the true
 257 positive rate (TPR) is 1. The overall accuracy is 86.4%, however, this includes misclassifications
 258 between the two negative, or non-event classes (“no signals” and “broadband signals”). The
 259 Heidke Skill Score (HSS) is 0.738.

260



261 Figure 2. An example spectrogram indicating the LoG identification circles. The smaller,
 262 unnumbered circles would be filtered out before event information (frequency and time ranges,
 263 pixel counts in each color bin) is extracted and recorded in a spreadsheet. This filtering is based
 264 on a user-set minimum radius threshold. Blobs 1 and 6 were not filtered out by the radius cutoff
 265 set in this case, since filtering these out would have also eliminated Blob 4, a weak EMIC event.
 266 This tradeoff must be optimized by the user for the desired results and specific dataset being
 267 analyzed. Blobs 2 and 3 indicate strong EMIC events. Blob 5 contains broadband signal, and as
 268 such is a misidentification. Since broadband signals are filtered out on a whole-spectrogram basis
 269 by the CNN classification, some spectrograms containing broadband are classified into the
 270 “EMIC event” class since they also contain large, strong events (such as in Blobs 2 and 3).

271

272 Table 1. Spreadsheet output from the LoG identification of the spectrogram in Figure 2. For each
 273 blob identified, the approximate time and frequency ranges are recorded, as well as numbers of
 274 pixels in each color bin corresponding to different power ranges. These pixel color counts, along
 275 with the total number of pixels in the blob, help the user to make rough estimates of event size
 276 and average power. The user can then decide which events are worth investigating further or
 277 including in additional analyses.

Blob ID	Approx. time range (hr)	Approx. freq. range (mHz)	Pixel counts in each color bin					Total # in blob	
			# white 10^{-1} to 10^0 nT ² Hz	# red 10^{-2} to 10^{-1} nT ² Hz	# orange 10^{-3} to 10^{-2} nT ² Hz	# yellow 10^{-4} to 10^{-3} nT ² Hz	# green 10^{-5} to 10^{-4} nT ² Hz		# blue, black 10^{-8} to 10^{-5} nT ² Hz
1	8-11	0-200	0	0	0	0	9	73	82
2	9-14	200-900	0	52	8	266	208	730	1264
3	14-18	200-800	0	3	5	172	200	386	766
4	19-21	400-600	0	0	0	1	16	116	133
5	21-24	300-700	0	0	0	22	119	299	440
6	22-24	0-200	0	0	0	0	4	133	137